Isken, M. P., Vasyura-Bathke, H., Dahm, T., Heimann, S. (2022): De-noising distributed acoustic sensing data using an adaptive frequency-wavenumber filter. - Geophysical Journal International, 231, 2, 944-949.

https://doi.org/10.1093/gji/ggac229

Geophysical Journal International

Geophys. J. Int. (2022) **231,** 944–949
Advance Access publication 2022 June 17
GJI Seismology

https://doi.org/10.1093/gji/ggac229

De-noising distributed acoustic sensing data using an adaptive frequency–wavenumber filter

Marius Paul Isken [1,2], Hannes Vasyura-Bathke [1,2], Torsten Dahm [1,2] and Sebastian Heimann[2]

[1] *GFZ German Research Centre for Geosciences, Telegrafenberg,* 14473 *Potsdam, Germany. E-mail: mi@gfz-potsdam.de*
[2] *Institute of Geosciences, University of Potsdam, Karl-Liebknecht-Str.* 24-25, 14476 *Potsdam, Germany*

Accepted 2022 June 15. Received 2022 April 29; in original form 2022 January 21

SUMMARY

Data recorded by distributed acoustic sensing (DAS) along an optical fibre sample the spatial and temporal properties of seismic wavefields at high spatial density. Often leading to massive amount of data when collected for seismic monitoring along many kilometre long cables. The spatially coherent signals from weak seismic arrivals within the data are often obscured by incoherent noise. We present a flexible and computationally efficient filtering technique, which makes use of the dense spatial and temporal sampling of the data and that can handle the large amount of data. The presented adaptive frequency–wavenumber filter suppresses the incoherent seismic noise while amplifying the coherent wavefield. We analyse the response of the filter in time and spectral domain, and we demonstrate its performance on a noisy data set that was recorded in a vertical borehole observatory showing active and passive seismic phase arrivals. Lastly, we present a performant open-source software implementation enabling real-time filtering of large DAS data sets.

Key words: Fourier analysis; Image processing; Time-series analysis; Seismic noise.

Key words:; Distributed acoustic sensing.

1 INTRODUCTION

Fibre optical distributed acoustic sensing (DAS) measures the strain rate along an optical fibre cable. The technique uses laser pulses to interrogate an optical fibre: a coherent light pulse is sent into the fibre and is reflected by impurities within the fibre. Amplitudes and phases of the reflected signal are measured by a photo diode. Through an interferometric method phase shifts are obtained and unwrapped to relative strain rate measurements at fixed gauge lengths along the optical fibre at nanometer precision (Blum *et al.* 2008; Lindsey *et al.* 2020). DAS data are sampled equidistantly, where spatial and temporal sampling rates are commonly on the order of several metres and few kHz, respectively. DAS can measure the axial strain rate along many kilometre long vacant dark telecommunication fibres or dedicated tight-buffered cables installed specifically for the purpose of optical seismic measurements.

DAS recordings provide a dense image of the spatial and temporal characteristics of the seismic wavefield and contain a wealth of information that can be used for a variety of applications, among them the study and monitoring of structures (e.g. buildings, pipelines, railway or airplanes), the recording of active and passive seismic sources for seismological and exploration geophysical application (e.g. earthquake detection or vertical seismic profiling; VSP), the monitoring of volcanic unrest and permafrost thaw, and the monitoring of urban traffic (Mateeva *et al.* 2012; Ajo-Franklin *et al.* 2017; Dou *et al.* 2017; Jousset *et al.* 2018; Bakhoum *et al.* 2020; Flóvenz *et al.* 2022; Tejedor *et al.* 2021; Gorshkov *et al.* 2022). Handling, organizing and exploring the vast amount of collected seismic data from a single measurement campaign can be a challenge for the established seismological workflow. Consequently, traditional seismological∗∗ tool-sets and methods have to be extended to extract valuable information from the spatially dense and high-frequency DAS data.

The quality and noise level of DAS recordings depend on many different factors and may vary along segments of the fibre. Noise sources include the noise environment of the installed optical instrument, optical and electronic noise, the reflectivity and quality of the optical fibre, splices and plugs, the ambient noise conditions along the fibre, or the coupling between the fibre and the ground (Hartog *et al.* 2014). Thus, the noise in DAS data can have different characteristics (broad-band or band-limited) and coherence between channels. 1-D time–frequency filters like Butterworth band-, low-

and high-pass filters are effective to suppress noise. Additionally, image processing anti-aliasing filters or range filters can be applied to the 2-D data set to remove unwanted noise, such as a median-filter (Huang *et al.* 1979). Machine learning techniques have been proposed for separating signal and noise in DAS data (e.g. Martin *et al.* 2018; van den Ende *et al.* 2021). Other approaches are inspired by methods adapted from active seismic exploration, where slant-stacking (radon transform of rank 1 or τ–p methods) have been used to enhance the signal-to-noise ratio (SNR, Kong *et al.* 1985; Schwarz *et al.* 2021). Optimization-based techniques to suppress coupling noise by continuous wavelet- and cosine-transformation have been presented by Chen *et al.* (2019).

The high spatial sampling of DAS measurements and the spatial coherence of the wavefield allows for spectral filtering techniques in the frequency–wavenumber (f–k)** domain. f–k filters are often used in active seismic exploration, such as the traditional f–k filter or adaptive f–k methods (Duncan & Beresford 1994). In this work, we introduce a modified adaptive Goldstein filter (Goldstein & Werner 1998) applied to a (nominal) f–k domain of dense linear DAS data in order to suppress energy of incoherent noise and to enhance the SNR. This adapted f–k filter technique is effective in enhancing the coherent signals in DAS recordings. It is computationally efficient such that it can be applied automatically on real-time acquisitions, and also interactively on existing data sets.

2 METHOD

2.1 Filter approach

The filter approach was first presented by Goldstein & Werner (1998) to enhance phase coherence in synthetic aperture radar (SAR) interferograms (InSAR) that are derived from SAR data acquired by satellites. The Goldstein filter technique is well established within the InSAR community to suppress uncorrelated noise in interferograms in 2-D spatial domain. The response of the adaptive Goldstein filter $H(u, v)$ applied to time–space domain of DAS data is

$$\mathcal{H}(u, v) = |\mathcal{E}(u, v)|^{\alpha} \cdot \mathcal{E}(u, v), \quad \text{with } u = f \text{ and } v = k. \tag{1}$$

While the filter works in the 2-D wavenumber space, $u = k_x$ and $v = k_y$, for interferograms; we use the f–k domain of the time and the linear-distance space for DAS strain-rate data (ε). We propose this application and the use of fast Fourier transformations (FFT), because DAS data are sampled equidistantly in t and x. If the DAS acquisition delivery is rectilinear, then k can be interpreted as the apparent spatial wavenumber of the wavefield along the direction of the cable. The filter technique works by sliding overlapping 2-D windows over the DAS data. Within independent windows $\varepsilon(t, x)$ the 2-D FFT $\mathcal{E}(f, k)$ is calculated and multiplied with its scaled amplitude spectrum $|\mathcal{E}(f, k)|^{\alpha}$. The scaling exponent $\alpha \in [0, 1]$ controls the strength of the filter, where 0 is no filtering and 1 is strong filtering. The convolution theorem states that the multiplication in the spectral domain is equivalent to a convolution in time-spatial domain. The multiplication with the scaled amplitude spectrum $|\mathcal{E}(f, k)|^{\alpha}$ enhances the energy of the large amplitude signals in f–k domain and thus amplifies the coherent components of the wavefield in time-spatial domain. The filter adapts to variations in the coherent wavefield such that windows with high coherence are filtered stronger than windows with low coherence. The sliding windows are quadratic of size n samples in linear space and time domain, and they have an overlap $n_o \leq n/2 - 1$. Optionally, rectangular windows of size n, m can be defined. The overlaps are tapered in t–x domain with a Bartlett (triangular) taper in order to fade equally between overlapping windows. Filtering in sliding windows makes the operation adapt to locally present coherent signals.

In the presented implementation we omit smoothing the amplitude spectrum, this approach was suggested by Goldstein & Werner (1998) and Baran *et al.* (2003) for InSAR data. Seismic data include signals in different frequency bands and wavenumbers; thus, smoothing the amplitude spectrum (particularly in a small window) distorts the signal amplitudes and narrows the filter band. The adaptive filter has a broadband characteristic, and is non-destructive, that is, it enhances the energy of coherent waves (wavenumbers) within individual filter windows and no energy will be suppressed to the stop band.

A weakness of eq. (1) is that the true amplitudes of the signal are lost. This can be partially accounted for by normalizing the amplitude spectrum coefficients (2). Doing so will retain the amplitude of the most dominant f–k component of the input.

$$\mathcal{H}(f, k) = |\mathcal{E}(f, k)|_N^{\alpha} \cdot \mathcal{E}(f, k), \tag{2}$$

where $|\mathcal{E}|_N = |\mathcal{E}| / \max |\mathcal{E}|$ is the normalized amplitude spectrum $\in [0, 1]$. In the following, we refer to the filters presented in eqs (1) and (2) as adaptive frequency–wavenumber (AFK) filter and as normalized adaptive frequency–wavenumber (NAFK) filter, respectively. The here introduced (N)AFK filters can be combined with traditional frequency filters, such as the low- and high-pass filters or Butterworth bandpass filters to further improve the SNR.

2.2 DAS data

As test data set, we use DAS data that were recorded in a vertical 400 m deep Eger Rift ICDP borehole in Landwüst, Germany (Dahm *et al.* 2013). The tight-buffer single-mode fibre optical cable is cemented behind the casing. The data were recorded with a commercial Silixa Ltd iDAS (version 2) interrogator with 10 m gauge length and 1 m channel spacing at 1 kHz sampling frequency. The data set includes a seismic signal excited by a 200 kg drop weight at 200 m distance to the well head, as well as body wave arrivals from a weak local earthquake (M_L1.0) in about 12 km distance (Fig. 1). The data show relatively high noise, because of large optical energy loss in the first metres of the fibre outside of the borehole. For compensation, the laser's energy was increased and the gain of the optical amplifier was elevated. Consequently, these measures introduced higher levels of noise on this short fibre.

3 RESULTS

We apply the AFK filter to the borehole DAS data containing the active signal (Fig. 1). The 2-D plots (Figs 1a–c) show the effect of the filter in time–space domain. A clear separation between the coherent wavefield and noise can be achieved. The residual (Fig. 1c) shows a reminiscence of the seismic signal due to the exaggerated dynamics of the filtered signal, particularly at steep signal flanks. This can also be seen in the exemplary waveform trace of channel 250 (Fig. 1d), where the successful suppression of noise prior to the arrival of the drop-weight signal can be seen. The signal's character is recovered, however, the relative amplitudes of the wave train are distorted by the AFK filter (eq. 1), which is why the raw and filtered data have been normalized to (− 1, 1) (Fig. 1d). In the following we quantify the noise reduction in terms of reduced spectral noise

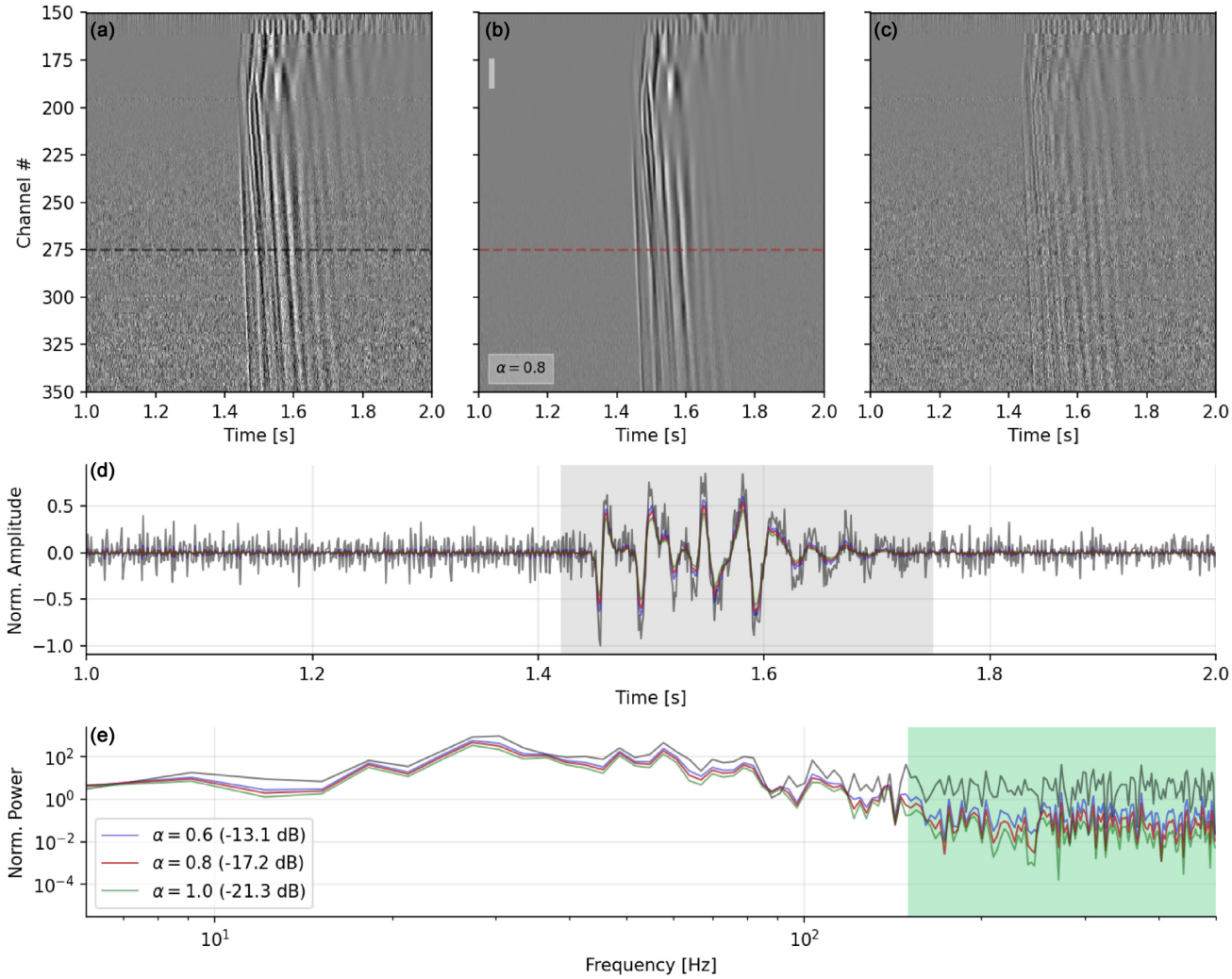

Figure 1. Active signal from a drop weight at 200 m distance to the 400 m deep vertical ICDP borehole in Landwüst, Germany. The figures show the performance of the AFK filter (eq. 1) applied to noisy DAS data. (a) Raw data with 1 kHz sampling frequency and 1 m channel spacing. (b) The filtered wavefield using the AFK filter with $\alpha = 0.6, 0.8, 1.0$, 32×32 sample window size n and 15 samples overlap. (c) The normalized residual between raw and filtered data. (d) Normalized raw (black) waveform and waveforms filtered (coloured) by different filter coefficients α recorded at channel 275, the shaded area marks the signal duration. (e) Power spectra of signal shown in (d; shaded duration), the green area covers the noise band used for estimating the reduction in spectral amplitude in dB. The data are neither tapered nor bandpass filtered, the images in (a)–(c) are not anti-aliased.

amplitudes in dB (Appendix A). The AFK filter suppresses high-frequency uncorrelated noise by −17.2 dB (at $\alpha = 0.8$ and $n = 32$) and preserves coherent energy from the traversing wavefield (Figs 1d and e). The closer the α parameter is to 1, the stronger the filtering will be. Lower values result in higher noise levels, but also correlated signals will be better preserved compared to the data filtered with higher alphas (Figs 1d and e).

For filter comparison, we apply the NAFK filter (eq. 2) to the same data with the same filtering parameters as shown in Fig. 1. In the 2-D data as well as in the waveforms (Figs 2a–d), a clear signal can be observed. Although, the noise energy outside the wavefield has overall higher amplitudes when compared with the AFK filter, the signal is emphasized above the background noise while the true amplitudes of the coherent signal are preserved. This effect is attributed to the adaptive and normalizing properties of the filter. While the AFK filter (eq. 1) increases the dynamic (contrast) between the coherent wavefield and uncorrelated background noise, thus improving the apparent SNR (eq. A.1, Supporting Information), the NAFK filter (eq. 2) is adaptive to the relative amplitude of the dominating local wavenumber (within the window). This property improves the local SNR within the passing coherent wavefield, thus recovering more details in wavefields with dynamic amplitudes (Fig. 2). However, the relative SNR improvement of the signal is worse with −8.8 dB (at $\alpha = 0.8$). The α parameter has little influence on the performance of the NAFK filter, that is, low and high values of α both lead to similar noise levels in filtered waveforms and spectra (Figs 2d and e). The N(AFK) filters perform similar when applied to recorded DAS data of a local earthquake (Appendix B, Figs A1 and A2, Supporting Information).

In Fig. A3 (Supporting Information), a synthetic wavefield of an inclined sweeping wavefield, simulating a changing slowness with added Gaussian spectral noise is shown after filtering with $\alpha = 0.8$ and different window sizes between 16×16 to 128×128 samples. It can be seen that larger filter windows show stronger edge effects and blur the signal (Appendix C). This shows the filter's leakage within large window sizes, leading to signal artefacts extending outside of the region of the signal. However, large windows are not required, even filter windows recover signals with wavelength larger than

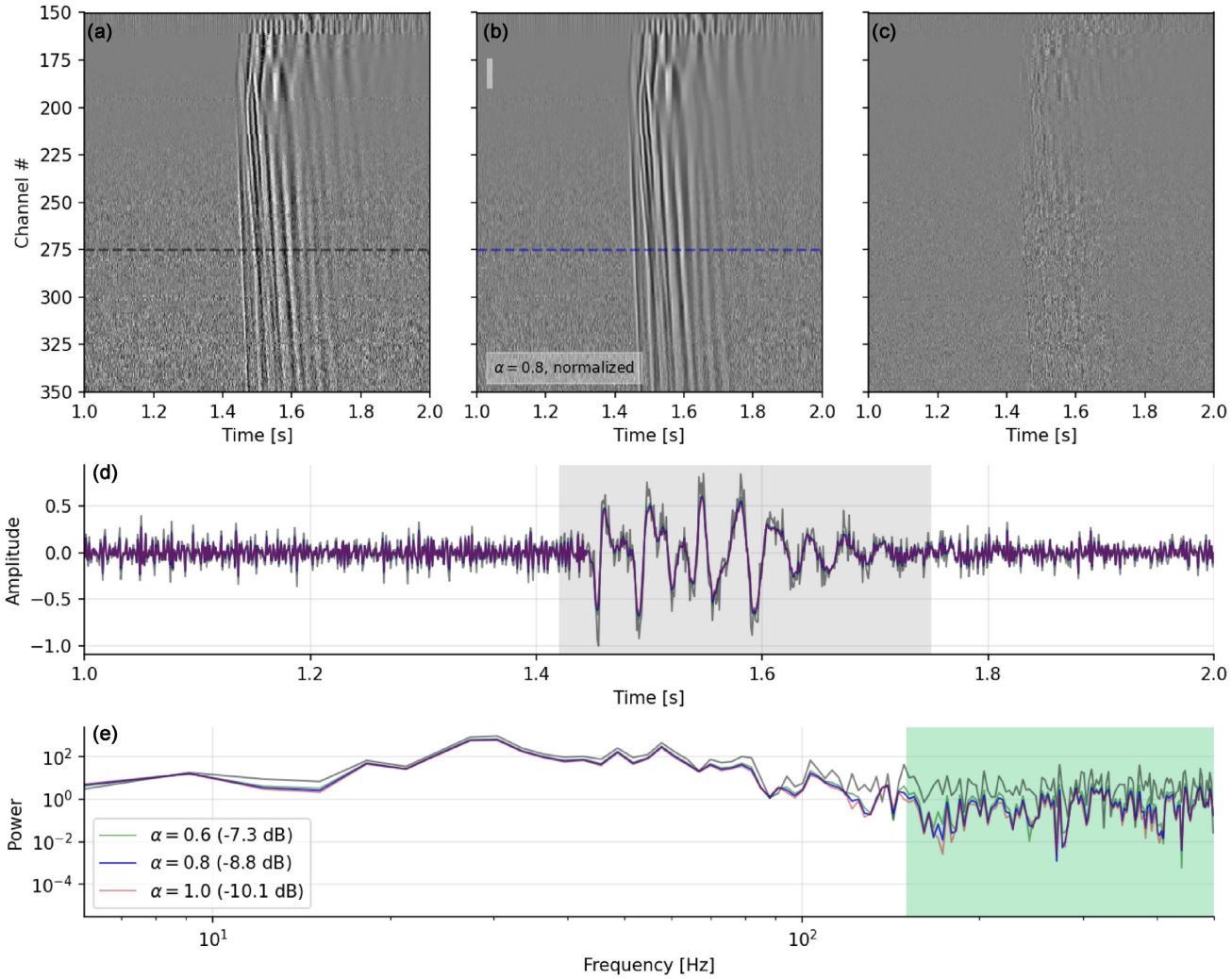

Figure 2. Active signal from a drop-weight source (see Fig. 1). The figures show the performance of the NAFK filter (eq. 2), applied to noisy DAS data. See caption of Fig. 1 for details.

the window. The filter's leakage with non-quadratic window sizes of different sizes is shown in Appendix D (Fig. A4, Supporting Information), where we apply the different filtering windows on recordings of a local earthquake. In conclusion, the window size in time should not exceed the period of the dominant waves in order to avoid filter leakage. The presented data have not been filtered in any other way and wavefield figures were created neither with anti-aliasing filters nor clipping of the colour map.

For comparison, we evaluate the performance of the (N)AFK filter against a neural network de-noiser (jDAS) (van den Ende *et al.* 2021, Fig. 3). The dynamic of the original signal has been better preserved by the AFK filter, however the NAFK filtered data shows higher background noise in time domain the signal and its coda is emphasized over the noise. The neural network filter introduces artefacts into the data, particularly the signal's coda and behaves erratic in spatial domain (Fig. 3d). Although some DAS channels may be completely noise dominated, the (N)AFK filters can use coherent energy of the neighboring channels to 'reconstruct' the signal.

The filter algorithm is implemented in the Rust system programming language (Matsakis & Klock 2014) with native bindings to Python (Van Rossum & Drake 2009). A data set of 4096×4096 samples (Fig. 3) can be filtered with a window size of 32×32 samples and maximum overlap in 0.03 s on a desktop workstation. Thus, this filter technique can be used in real-time applications. For comparison, a neural network approach applied to the same data set required 7.2 s on the same workstation (Figs 3a and c). The presented filter is part of the open-source lightguide toolbox (Isken *et al.* 2022a) and is implemented into the Pyrocko's Snuffler App (Heimann *et al.* 2017), an interactive waveform and wavefield explorer. It is to note that the computational performance of the filter depends on the size and subsequent number of the independent filtering windows.

4 DISCUSSION AND CONCLUSIONS

The coherent wavefield recorded in the DAS data can be successfully separated from the incoherent noise by both presented filter variants. While the AFK filter better suppresses uncorrelated noise it distorts the signal's amplitudes. The NAFK filter does suppress uncorrelated noise within correlated signals less effectively, but it maintains the true amplitude of the seismic wavefield. The filter's application and strength lies in emphasizing and recovering a coherent wavefield, and thus can aid interpretation and analysis of the

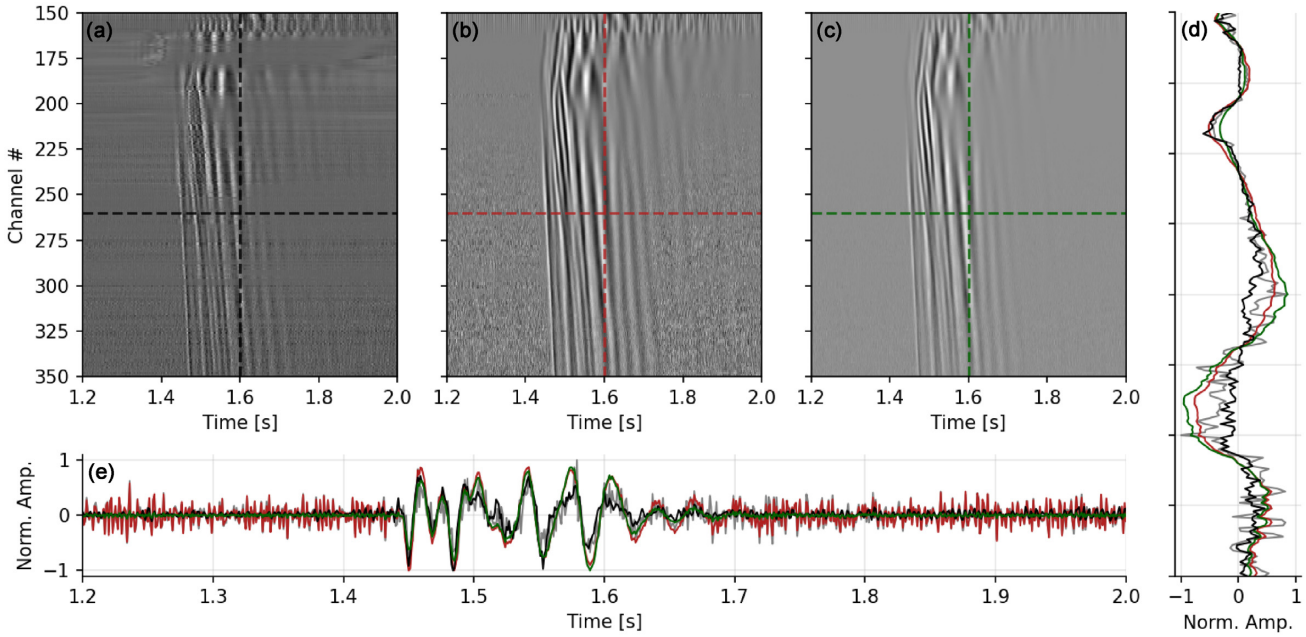

Figure 3. Comparison of the NAFK filter against a neural network de-noiser (jDAS, van den Ende *et al.* 2021). DAS data de-noised with (a) jDAS, (b) the NAFK filter and (c) the AFK filter. For the N/AFK filter $\alpha = 0.8$, the window size is 32 samples with 15 samples overlap. (d) Vertical slice across the channels comparing jDAS (black), N/AFK filter (red/green lines) and raw data (gray) at $t = 1.6$ s. In (e), the channel 260 of the jDAS (black) and N/AFK (red/green lines) filtered data is shown as time-series, the unfiltered raw data are shown in grey. The pre-trained jDAS network has been used and no post-filtering has been applied to either data set.

seismic data. These filters are attractive for routine processing of large DAS data sets due to their robustness, computational performance and small number of parameters. When the filters are applied conservatively (small window size and small α) little to no artefacts are introduced to the data, whereas large window sizes in x and t can introduce acausal leakage and ringing due to spreading the amplified energy of dominating wavenumbers (Fig. A4, Supporting Information). The non-destructive broadband character of the filters enables a wide variety of seismological and seismic applications, especially when combined with established frequency band filtering techniques.

The filters' performance and computational efficiency is outperforming recent neural-network approaches for de-noising DAS data (Fig. 3), furthermore, the sturdy *f–k* approach does not require retraining of a neural network (on a fixed-size data frame) for new data sets or changing noise environments. The presented technique is purely data-driven and leverages well-known signal-processing techniques for DAS data. The real-time performance of the filter allows to control its parameters (i.e. strength α and window size) interactively, thus enabling the interactive exploration of the recorded seismic wavefields (as implemented in the Pyrocko toolbox). The small and independent filtering windows allow the filter to work on data acquired along undulating cable geometries with rapidly changing apparent slowness of the wavefield. Both, the AFK and the NAFK filters are potentially suitable for a wider application in evenly spaced geophysical data sets. While the AFK filter is very effective in the suppression of uncorrelated noise, it is limited to applications where the signal amplitudes themselves are not important, for example, event detection and localization, ambient noise correlation, earthquake clustering, active seismic surveying or for imaging with ground-penetrating radar. The NAFK filter is suitable to suppress noise in applications where signal amplitudes are important, for example, earthquake source inversions or rupture directivity studies.

ACKNOWLEDGMENTS

The VSP experiment in Landwüst was supported by Christopher Wollin, Charlotte Krawczyk and Philippe Jousset from GFZ Potsdam (Section 2.2) who also provided the Silixa iDAS v2 interrogator. The drop weight for the VSP shots was provided by the GIPP pool at GFZ Potsdam. The plots have been generated using Matplotlib (Hunter 2007) and Pyrocko (Heimann *et al.* 2017). The high-performance filter functions are leveraging the discrete Fourier transforms from the FFTW package and the filter has been implemented in Rust system programming language (Matsakis & Klock 2014). This work was funded by the DEEPEN project (GEOTHERMICA; Bundesministerium für Wirtschaft und Energie, Germany, funding no. 03EE4018). The raw DAS data were converted to MiniSEED with DAS convert (Isken *et al.* 2021).

DATA AVAILABILITY

All data shown and analysed as well as the software are openly available. The software package and filter implementation is part of the Python package *lightguide* and can be downloaded from Pyrocko git repositories at https://github.com/pyrocko/lightguide. All shown DAS data sets and plotting scripts are part of the extended electronic supplement published through Zenodo, see Isken *et al.* (2022b). The jDAS neural network is provided by van den Ende *et al.* (2021) at https://github.com/martijnende/jDAS..

REFERENCES

Ajo-Franklin, J. *et al.*, 2017. Time-lapse surface wave monitoring of permafrost thaw using distributed acoustic sensing and a permanent automated seismic source, in *SEG Technical Program Expanded Abstracts 2017,* pp. 5223–5227, Society of Exploration Geophysicists.

Bakhoum, E.G., Zhang, C. & Cheng, M.H., 2020. Real time measurement of airplane flutter via distributed acoustic sensing, *Aerospace,* **7**(9), 125.

Baran, I., Stewart, M.P., Kampes, B.M., Perski, Z. & Lilly, P., 2003. A modification to the goldstein radar interferogram filter, *IEEE Trans. Geosci. Remote Sens.,* **41**(9), 2114–2118.

Blum, J.A., Nooner, S.L. & Zumberge, M.A., 2008. Recording earth strain with optical fibers, *IEEE Sens. J.,* **8**(7), 1152–1160.

Chen, J., Ning, J., Chen, W., Wang, X., Wang, W. & Zhang, G., 2019. Distributed acoustic sensing coupling noise removal based on sparse optimization, *Interpretation,* **7**(2), T373–T382.

Dahm, T., Hrubcová, P., Fischer, T., Horálek, J., Korn, M., Buske, S. & Wagner, D., 2013. Eger rift icdp: an observatory for study of non-volcanic, mid-crustal earthquake swarms and accompanying phenomena, *Sci. Drill.,* **16,** 93–99.

Dou, S. *et al.*, 2017. Distributed acoustic sensing for seismic monitoring of the near surface: a traffic-noise interferometry case study, *Sci. Rep.,* **7**(1), 1–12.

Duncan, G. & Beresford, G., 1994. Slowness adaptive fk filtering of prestack seismic data, *Geophysics,* **59**(1), 140–147.

Flóvenz, Ó. *et al.*, 2022. Cyclical geothermal unrest as a precursor to Iceland's 2021 Fagradalsfjall eruption., *Nature Geoscience,* **15**(5), 397–404, EGU General Assembly Conference Abstracts.

Goldstein, R.M. & Werner, C.L., 1998. Radar interferogram filtering for geophysical applications, *Geophys. Res. Lett.,* **25**(21), 4035–4038.

Gorshkov, B.G. *et al.*, 2022. Scientific applications of distributed acoustic sensing: state-of-the-art review and perspective, *Sensors,* **22**(3) , doi:10.3390/s22031033.

Hartog, A., Frignet, B., Mackie, D. & Clark, M., 2014. Vertical seismic optical profiling on wireline logging cable, *Geophys. Prospect.,* **62,** 693–701 (4-Vertical Seismic Profiling and Microseismicity Frontiers).

Heimann, S. *et al.*, 2017. Pyrocko-an open-source seismology toolbox and library.

Huang, T., Yang, G. & Tang, G., 1979. A fast two-dimensional median filtering algorithm, *IEEE Trans. Acoust. Speech Signal Process.,* **27**(1), 13–18.

Hunter, J.D., 2007. Matplotlib: a 2d graphics environment, *Comput. Sci. Eng.,* **9**(03), 90–95.

Isken, M.P., Wollin, C., Heimann, S., Quinteros, J., Jäckel, K.-H. & Jousset, P., 2021. *DAS Convert-convert Distributed Acoustic Sensing Data. v. 1.0*.

Isken, M.P., Heimann, S., Wollin, C., Bathke, H. & Dahm, T., 2022a. *Lightguide—Seismological Tools for DAS Data* , doi:10.5281/zenodo.6580579.

Isken, M.P., Vasyura-Bathke, H., Heimann, S. & Dahm, T., 2022b. *Extended Supplement for De-noising Distributed Acoustic Sensing Data using an Adaptive Frequency-Wavenumber Filter* , doi:10.5281/zenodo.6485993.

Jousset, P. *et al.*, 2018. Dynamic strain determination using fibre-optic cables allows imaging of seismological and structural features, *Nat. Commun.,* **9**(1), 1–11.

Kong, S.M., Phinney, R.A. & Roy-Chowdhury, K., 1985. A nonlinear signal detector for enhancement of noisy seismic record sections, *Geophysics,* **50**(4), 539–550.

Lindsey, N.J., Rademacher, H. & Ajo-Franklin, J.B., 2020. On the broadband instrument response of fiber-optic DAS arrays, *J. geophys. Res.: Solid Earth,* **125**(2), 1–16.

Martin, E.R., Huot, F., Ma, Y., Cieplicki, R., Cole, S., Karrenbach, M. & Biondi, B.L., 2018. A seismic shift in scalable acquisition demands new processing: fiber-optic seismic signal retrieval in urban areas with unsupervised learning for coherent noise removal, *IEEE Signal Process. Mag.,* **35**(2), 31–40.

Mateeva, A. *et al.*, 2012. Advances in distributed acoustic sensing (DAS) for VSP, in *SEG Technical Program Expanded Abstracts 2012,* pp. 1–5, Society of Exploration Geophysicists.

Matsakis, N.D., Klock & F.S. II, 2014. The rust language, in *ACM SIGAda Ada Letters,* Vol. **34,** pp. 103–104, ACM.

Schwarz, B., Sager, K., Jousset, P., Currenti, G., Krawczyk, C. & Tsai, V., 2021. Leveraging coherent wave field analysis and deep learning in fiber-optic seismology, in *EGU General Assembly Conference Abstracts,* pp. EGU21–7856.

Tejedor, J., Macias-Guarasa, J., Martins, H.F., Martin-Lopez, S. & Gonzalez-Herraez, M., 2021. A multi-position approach in a smart fiber-optic surveillance system for pipeline integrity threat detection, *Electronics,* **10**(6) , doi:10.3390/electronics10060712.

van den Ende, M. P.A., Lior, I., Ampuero, J.-P., Sladen, A., Ferrari, A. & Richard, C., 2021. *A Self-supervised Deep Learning Approach for Blind Denoising and Waveform Coherence Enhancement in Distributed Acoustic Sensing Data* , doi:10.31223/X55K63.

Van Rossum, G. & Drake, F.L., 2009. *Python 3 Reference Manual,* CreateSpace, Scotts Valley, CA.

SUPPORTING INFORMATION

Supplementary data are available at *GJI* online.

Figure S1. Noisy record of a regional earthquake event M_L 4 in Poland at 300 km distance to the ICDP borehole in Landwüst, Germany. Performance of the AFK filter (eq. 1). See the caption of Fig. 1 for details.

Figure S2. Noisy record of a regional earthquake event, see Fig. A1 for event details. Performance of the NAFK filter (eq. 2). See captions of Fig. 1 and Fig. A1 for further details.

Figure S3. Synthetic test with a sweeping wavefield expressing different slowness, overlaid by Gaussian spectral noise. The sampling is regular at 1 m at 100 Hz, the linear sweep as a function of×is from 0.1 to 2 Hz. The filter exponent $\alpha = 0.8$ for four different filter sizes (32, 64, 128 and 256 samples at maximal overlap) for the AFK (second row) and NAFK filter (third row) type are shown. The white rectangle shows the size of the filter window. The lower panels show the averaged and normalized power spectra of the signal region for the input (black), AFK (red) and NAFK filter (blue). The green area shows the noise frequency band used for calculating the filter effect in dB.

Figure S4. Wavefield from a local earthquake (M_L 1 at 12 km hypocentre distance) recorded on the vertical DAS fibre in the ICDP borehole in Landwüst, Germany. Comparison of rectangular window sizes using the NAFK filter. The white rectangle in the lower left corner shows the different window sizes, from top to bottom: 16 traces×0.05 s, 16 traces×0.1 s, 32 traces×0.2 s and 32 traces×0.4 s. The white dashed line at 14.1 s illustrates the *P*-phase arrival time at channels 336 to 660, and serves as a visual anchor to demonstrate leakage of large windows. The coherent wavefield shows increasing leakage of the filter illustrated through apparent wave arrivals even before the *P*-phase arrival with growing filter window sizes. The figures have been plotted without interpolation.

Please note: Oxford University Press is not responsible for the content or functionality of any supporting materials supplied by the authors. Any queries (other than missing material) should be directed to the corresponding author for the paper.